NJC

Accepted Manuscript

This is an *Accepted Manuscript*, which has been through the Royal Society of Chemistry peer review process and has been accepted for publication.

Accepted Manuscripts are published online shortly after acceptance, before technical editing, formatting and proof reading. Using this free service, authors can make their results available to the community, in citable form, before we publish the edited article. We will replace this *Accepted Manuscript* with the edited and formatted *Advance Article* as soon as it is available.

You can find more information about *Accepted Manuscripts* in the Information for Authors.

Please note that technical editing may introduce minor changes to the text and/or graphics, which may alter content. The journal's standard Terms & Conditions and the Ethical guidelines still apply. In no event shall the Royal Society of Chemistry be held responsible for any errors or omissions in this *Accepted Manuscript* or any consequences arising from the use of any information it contains.

ROYAL SOCIETY OF CHEMISTRY

www.rsc.org/njc

Journal Name

RSCPublishing

ARTICLE

Synthesis of robust hierarchically porous zirconium phosphate monolith for efficient ion adsorption

Cite this: DOI: 10.1039/x0xx00000x

Yang Zhu,[a] Taiyo Shimizu,[a] Takara Kitajima,[b] Kei Morisato,[c] Nirmalya Moitra,[a] Nicolas Brun,[a] Tsutomu Kiyomura,[d] Kazuyoshi Kanamori,[a]* Kazuyuki Takeda,[a] Hiroki Kurata,[d] Masamoto Tafu,[b] and Kazuki Nakanishi[a]*

Received 00th January 2012,
Accepted 00th January 2012

DOI: 10.1039/x0xx00000x

www.rsc.org/

Hierarchically porous monolithic materials are advantageous as adsorbent, catalyst and catalyst support due to the better accessibility of reactants to active sites and the ease for recycle and reuse. Traditional synthetic routes, however, find their limitations in designing the hierarchical porosity as well as the mechanically stable monolithic shape in inorganic phosphate materials, which are useful as adsorbent and catalyst. We herein present a low-temperature, one-step liquid phase synthesis of hierarchically porous zirconium phosphate (ZrP) monoliths with tunable compositions (from $Zr(HPO_4)_2$ (Zr:P = 1:2) to NaSICON (Na super ionic conductor)-type ZrP (Zr:P = 1:1.5)) as well as macropore size (from 0.5 to 5 μm). The as-synthesized ZrP monolith with high reactive surface area (600 m^2 g^{-1}) and relatively high mechanical strength (Young's modulus 320 MPa) has been applied to ion adsorption. A simple syringe device inserted tightly with the ZrP monolith as a continuous flow setup has been demonstrated to remove various toxic metal ions in aqueous solution, which shows promising results for water purification.

Introduction

Discovery and design of materials hold the keys to many significant issues such as energy shortage and environmental pollution, which have been becoming increasingly problematic in the sustainable development of modern societies. Versatility, as a well-established concept for the synthesis and design of new materials, is being more emphasized in recent material research. The design concept includes the development of clean, facile and sustainable methods for the synthesis of new materials through simultaneous controls over the structural and chemical properties for various applications.

Zirconium phosphate (ZrP) has been focused as a multifunctional material. Since its first report on synthesis in the laboratory scale and the ion exchange behavior by Clearfield and colleagues,[1,2] ZrP has been attracting a great deal of interest due to its extended applications in various possible utilizations such as catalyst and catalyst support for different chemical reactions,[3,4] proton conductor for fuel cells,[5,6] and ion exchanger for water purification.[7,8] As an acidic layered compound, ZrP and its analogues such as sodium zirconium phosphate stands out by their high structural stability. Interestingly, the stability was also proven for nuclear radiations, which would extend its application to the solidification of nuclear wastes.[8,9]

In order to satisfy the requirements for applications in different fields, ZrP has been prepared into different morphologies, such as mesoporous (2-50 nm) and microporous (< 2 nm) particles and thin films via liquid phase synthesis.[10-12] However, to the best of our knowledge, no research has focused on the liquid-phase preparation of monolithic macroporous (> 50 nm) metal(IV) phosphates, let alone ZrP. This is partially due to their low solubility in liquid phase, which leads, in most of the cases, to ineluctable precipitation and difficult structurization to impart desirable porosity. Macroporous monoliths, compared with particles and thin films, are more easily reusable. Particularly, as already demonstrated in literature, fluids can be continuously transported through the monoliths, which are then recovered for repetitive uses.[13-17] The potentially high mechanical strength of monoliths against back pressure makes them prospective candidates in various fields such as separation science[18-20] and environmental and biological applications.[21,22] In order to form a monolithic material with homogeneous porous structure, a continuous network with sufficient mechanical strength should be formed during the transition from a homogeneous liquid to a structuralized gel. In the case of ZrP, however, precipitates tend to form in most of the solvents and in a wide pH range when precursors are mixed together as mentioned above. Recently Carn et al. reported the synthesis of monolithic macrocellular foam of ZrP by an air-liquid foam shaping method. Despite the control of macropore size and wall thickness, the skeleton formed by highly crystalline particles with low connectivity led to the low mechanical properties of the monolith, which limited its application.[23] Hence, for metal(IV) phosphates, such as ZrP, as an important member in the family of inorganic materials, it

still remains as a challenge in controlling macropores or even hierarchical porous structure in the monoliths with sufficient mechanical strength, which will bring new functions to these old materials and extend their applications into new fields. In this research, as the first attempt, a hierarchically porous ZrP monolith combining micrometer order macropores and nanometer order mesopores has been successfully synthesized. The hierarchically porous structure has been obtained as a result of structurization by phase separation (spinodal decomposition) during the sol-gel transition. A continuous flow set-up has been established by using the obtained ZrP monolith showing promising performances for the removal of various cationic pollutants from aqueous solutions.

Experimental

Reagents

Zirconium oxychloride hexahydrate (Wako Pure Chemicals Ind., Ltd., Osaka, Japan) as the zirconium source and concentrated phosphoric acid (≥85 wt% in H_2O, Sigma-Aldrich Co. USA) as the phosphate source were used. Mixture of distilled water (Hayashi Pure Chemicals Ind., Co., Ltd., Japan), hydrochloric acid (Kishida Chemical, Japan) and glycerol (Kishida Chemical, Japan) was used as the solvent. Both poly(ethylene glycol) (PEO, average molecular weight 35,000, Sigma-Aldrich Co., USA) and polyacrylamide (PAAm, average molecular weight 10,000, 50 wt% in H_2O, Sigma-Aldrich Co., USA) were used as the phase-separation inducers. Xylose (Tokyo Chemical Industry Co., Ltd., Japan) was used as the reactant in the dehydration reaction and furfural (Tokyo Chemical Industry Co., Ltd., Japan) was used for calibration of the product. CsCl, $SrCl_2{\cdot}6H_2O$, $Pb(NO_3)_2$, $Cd(NO_3)_2{\cdot}4H_2O$ (Kishida Chemical, Japan) and $AgNO_3$, $ZnCl_2$, $CuCl_2{\cdot}2H_2O$, $FeCl_3{\cdot}6H_2O$ (Sigma-Aldrich Co., USA) were used for the ion adsorption experiments. All the reagents were of analytical grade and used as received without further purification.

Synthesis of ZrP monoliths

The typical monolithic ZrP gel with hierarchically porous structure was synthesized by the following procedure. First, 1.29 g of zirconium oxychloride hexahydrate was dissolved in the mixture of 1.4 mL of 1 M hydrochloric acid and 1.6 mL of glycerol in a glass bottle. Predetermined amounts of PEO (W_{PEO}) and PAAm (W_{PAAm}) were then added to the solution (details are shown in Table 1). The mixture was kept stirred until a clear transparent solution was obtained, and the solution was then cooled at 0 °C in an ice-water bath. Then, a predetermined amount of concentrated phosphoric acid (V_{H3PO4}) that had been already cooled at 0 °C was added. The resultant solution was kept stirred for 5 min, followed by gelation at 0 °C. The resultant wet gel was aged at room temperature for 24 h, solvent-exchanged with 2-propanol for 3 times (more than 12 h for each time) and dried with supercritical CO_2 at 80 °C and 14 MPa. The name of the sample was denoted as ZrP-W_{PEO}-W_{PAAm}-V_{H3PO4}.

Ion adsorption by ZrP monolith

In order to evaluate the removal efficiency of ions in aqueous solution, the ZrP monolith (see detailed size information about the sample in Table SI1, in the Supporting Information) was first wrapped with parafilm and fitted into a 10 mL syringe with the inner diameter of 16 mm. Then, 2 mL of water was introduced into the syringe to wet the monolith. A tight fitting of the monolith is ensured by slight swelling of the monolith and a buffering effect of the parafilm.

The ion adsorption experiment was conducted by flowing a series of metal salt (CsCl, $AgNO_3$, $SrCl_2$, $CuCl_2$, $NiCl_2$, $Pb(NO_3)_2$, $Cd(NO_3)_2$, $ZnCl_2$, $NiCl_2$) solution (10 mM, 10 mL) into the syringe with a syringe pump. The flow rate was set at 0.2 mL/min. The treated solution from the outlet was collected with a beaker and subjected to the inductively coupled plasma-optical emission spectroscopy (ICP-OES) measurement. Due to the high concentration of metal salt, the original solutions were diluted 20 times with nitric acid for ICP-AES measurements, while the solutions after adsorption were measured without dilution.

Characterizations

Morphology of the fractured surface of the samples and the chemical compositions were investigated by scanning electron microscopy-energy dispersive X-ray spectroscopy (SEM-EDS, JSM-6060S, JEOL, Japan), field emission scanning electron microscopy (FE-SEM, JSM-6700F, JEOL, Japan) and transmittance electron microscopy (TEM, JEM-2200FS, JEOL, Japan) equipped with a spherical aberration corrector (CEOS, CETCOR). The crystal structure was confirmed by powder X-ray diffraction (XRD, RINT Ultima III, Rigaku Co., Japan) using Cu K_α (λ = 0.154 nm) as an incident beam. Thermal properties of the samples were investigated by thermogravimetry-differential thermal analysis (TG-DTA, Thermal Plus TG 8120, Rigaku Co., Japan) with a continuous air supply at 100 mL/min. The samples for TG-DTA were the concentrated liquid phase dried at 80 °C for 72 h (the solvent-rich phase as a result of the phase separation) and the as-dried ZrP gel (gel-rich phase) obtained after washing. Fourier transform infrared spectroscopy (FT-IR, IR Affinity-1, Shimadzu Co., Japan) and elemental analysis were performed to confirm the molecular and atomic level information. The molecular-level environments of phosphor in the monolith were revealed by solid-state ^{31}P dipolar decoupled magic angle spinning (DDMAS) NMR performed at room temperature in a magnetic field of 7 T on an OPENCORE NMR spectrometer[24,25] with a 5 mm MAS probe. The carrier frequency and the sample spinning frequency for ^{31}P were 121.249 MHz and 10 kHz, respectively, and the contact time was 2 ms. Meso- and microstructure of the samples were characterized by nitrogen adsorption-desorption (BELSORP-mini II, Bel Japan Inc., Japan). Skeletal density and mechanical property of the sample were investigated by a pycnometer (ULTRAPYC 1200e, Quantachrome Corp., USA) and a material tester (EZGraph, Shimadzu Corp., Japan), respectively.

The quantitative measurement of ion concentration before and after ion adsorption was determined by ICP-OES (Varian 720-ES, Agilent Technology Inc., U.S.). Calibration was carried out with the standard solutions of the elements.

Results and discussion

Synthesis of macroporous ZrP monoliths

The starting compositions are listed in Table 1. Both zirconium oxychloride and concentrated phosphoric acid are frequently used as zirconium and phosphate sources, respectively, for the synthesis of zirconium phosphate and related materials.[1,26] Aqueous solution of hydrochloric acid (1 M) and glycerol were chosen as the solvents to prevent precipitation after the addition

of concentrated phosphoric acid. Two water-soluble polymers, PAAm and PEO, are used to induce phase separation in the sol-gel processings.[27,28] Figure 1 shows SEM images of the ZrP monoliths prepared with different amounts of PEO (with a constant amount of PAAm) and different amounts of PAAm (with a constant amount of PEO), respectively. Figure 1D shows the appearance of a crack-free gel obtained after supercritical drying. The addition of only a single kind of polymer leads to the formation of monolithic gels with small particle aggregation without macropores in the micrometer scale, and macroporous co-continuous structure was obtained only when both polymers were added together into the starting solution. By increasing the amount of one polymer while keeping the other constant, the macroscopic morphology changes from small particle aggregates to macroporous co-continuous structure, then to spherical large particle aggregates (with excess PEO) (Figure 1A, B, C, E) or isolated macroporous structure (with excess PAAm) (Figure 1F, F, C, H). The macropore size can be controlled from 0.5 μm to 5 μm simply by varying the amount of polymers (Figure 1 and SI1, ESI†), enabling the application of ZrP monolith for multiple purposes that require different pore sizes.

Table 1 Starting compositions of ZrP monoliths

Sample[a]	W_{PEO}/g	W_{PAAm}/g	V_{H3PO4}/mL
ZrP-0-0.2-0.55	0	0.2	0.55
ZrP-0.05-0.2-0.55	0.05	0.2	0.55
ZrP-0.06-0.2-0.55	0.06	0.2	0.55
ZrP-0.12-0.2-0.55	0.12	0.2	0.55
ZrP-0.06-0-0.55	0.06	0	0.55
ZrP-0.06-0.15-0.55	0.06	0.15	0.55
ZrP-0.06-0.38-0.55	0.06	0.38	0.55
ZrP-0.065-0.23-0.55	0.065	0.23	0.55
ZrP-0.06-0.2-0.27	0.06	0.2	0.27
ZrP-0.06-0.2-0.41	0.06	0.2	0.41
ZrP-0.06-0.2-1.09	0.06	0.2	1.09

[a] The amount of $ZrOCl_2 \cdot 8H_2O$, 1 M HCl solution and glycerol are 1.29 g, 1.4 mL and 1.6 mL, respectively, for all the samples.

According to our previous research, the phase relation of a gelling mixture with two polymers is largely determined by their molecular weight and the chemical affinity between them.[29] To clarify the roles of the two polymers in the system, thermal analysis by TG-DTA was carried out. Such analysis allows understanding of the preferential distribution of both polymers between the gel-rich and the solvent-rich phases during the phase separation. Obtained TG-DTA curves are shown in Figure 2A and B. The endothermic peak accompanied by a weight loss from 100 °C to 220 °C in the TG-DTA curve of the concentrated solvent-rich phase can be attributed to the evaporation of glycerol. It has to be noticed that no such thermal event could be found in the TG-DTA curve of the gel-rich phase, which means that most of the glycerol added to the system distributes in the solvent-rich phase. Meanwhile, the decomposition of PAAm is observed only in the TG curve of the gel-rich phase with the weight loss occurring in the range from 300 °C to 400 °C. Such feature indicates that PAAm is preferentially distributed in the gel-rich phase. Similar results were obtained from FT-IR analyses. In FT-IR spectra, the broad and strong peak at 1062 cm^{-1} and the two peaks at 517 cm^{-1} and 609 cm^{-1}, which were found in all the spectra in Figure 2C, can be attributed to the stretching of P-O bands and the deformation bands of phosphate groups, respectively.[30] Resolved peaks at 1666 cm^{-1} together with the small peak at 1400 cm^{-1} related to the bending and deformation vibrations of N-H bonds are observed in the spectra of dried ZrP gels synthesized with PAAm (Figure 2C(3) and 2C(4)).[31] These results are in agreement with the observations from TG-DTA measurements, supporting that PAAm is preferentially distributed to the gel-rich phase.

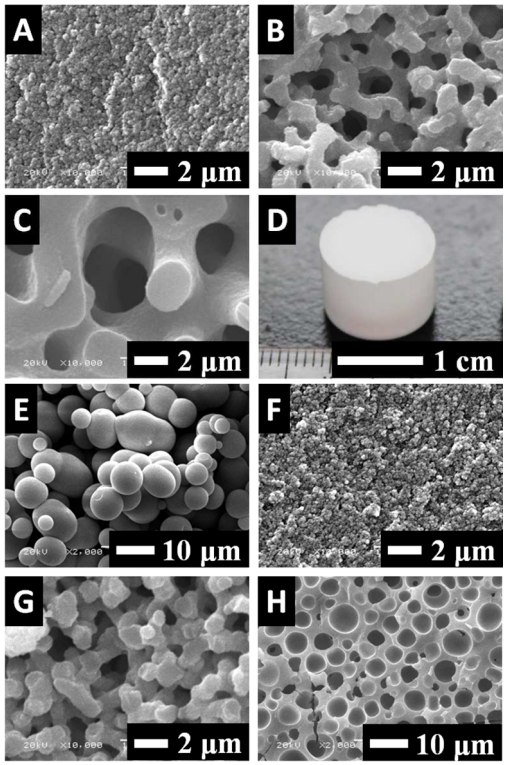

Figure 1. SEM images of monolithic ZrP monoliths; ZrP-0-0.2-0.55 (A), ZrP-0.05-0.2-0.55 (B), ZrP-0.06-0.2-0.55 (C), ZrP-0.12-0.2-0.55 (E), ZrP-0.06-0-0.55 (F), ZrP-0.06-0.15-0.55 (G), ZrP-0.06-0.38-0.55 (H) and the appearance of supercritically-dried gel of ZrP-0.06-0.2-0.55 (D).

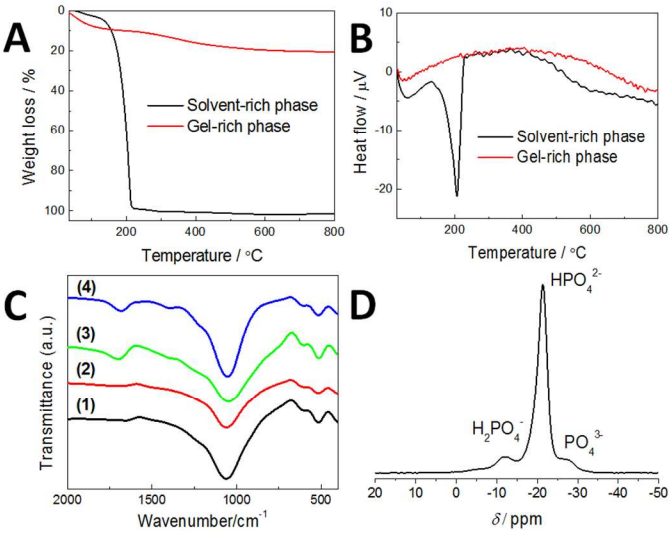

Figure 2. TGA curves (A) and DTA curves (B) of the solvent-rich phase (black curve), and the gel-rich phase (red curve, the amounts of polymers added: PEO 0.06 g, PAAm 0.2 g), FT-IR spectra of ZrP monoliths synthesized without the addition of polymers (1), with the addition of either PEO (2) or PAAm (3) and both PEO and PAAm (4) (C), ^{31}P-MAS NMR spectrum of ZrP monolith synthesized with the addition of both PEO and PAAm (D).

After mixing all the starting reagents including two polymers, there possibly undergo two kinds of condensation reactions; condensation between -Zr-OH and -P-OH and condensation between two -Zr-OH species. In hydrochloric acid solution with pH < 1, however, it is known that zirconium tends to stay in the form of cationic hydroxo complex.[32] Since the starting pH in the present system is lower than 1 (1 M HCl as the solvent), the condensation between -Zr-OH and -P-OH would be dominant to form a Zr-O-P network. Nevertheless, the rate of the condensation reaction between zirconium species and phosphoric acid is not too high due to the steric hindrance by PAAm attached to zirconium species through the strong coordination effects of amide groups and the high viscosity of the solution containing glycerol. Sol-gel transition therefore occurs in a controlled manner as the homogeneous condensation reaction of ZrP oligomers proceeds. Meanwhile, as PEO has no apparent interaction with Zr-O-P networks, it is assumed to distribute to both phases. The degree of polymerization reduces the compatibility between the polymerizing P-O-Zr-PAAm network and the PEO-containing solvent, which leads to the phase separation. The phase separation tendency becomes higher with increasing amount of PEO, and with an excess amount of PEO, too high phase separation tendency leads to the formation of spherical particles before gelation due to the reduction of surface tension of the gelling phase (Figure 1E). On the other hand, since PAAm is preferentially distributed to the gel-rich phase, the increase of the amount of PAAm with the constant amount of PEO increases the volume fraction of the gel-rich phase. Therefore, when an excess amount of PAAm is added, monoliths with isolated macropores are obtained (Figure 1H). Without the presence of either PEO or PAAm in the system, thermodynamic immiscibility between the P-O-Zr-PAAm network and the solvent or P-O-Zr network and PEO-containing solvent is not high enough for the phase separation to be induced during the sol-gel transition (Figure 1A, F). In a word, the addition of both PEO and PAAm increases the overall enthalpy by increasing the incompatibility between the solvent-rich and gel-rich phases together with the loss of entropy due to the polymerization of P-O-Zr network. Phase separation occurs because the change in Gibbs free energy of mixing becomes positive in such thermodynamic system, and it gives rise to the formation of co-continuous macroporous structure.

Detailed compositional information of ZrP monolith was revealed by EDS, elemental analysis and ^{31}P DDMAS NMR. The molar ratio of Zr to P obtained from EDS is 1 to 2, which is consistent with the ratio in both precursors. The lack of unreacted phosphoric acid is confirmed by the absence of any signal at 0 ppm in the ^{31}P DDMAS NMR spectrum of ZrP monolith. The appearance of three resolved resonance peaks at −12 ppm, −21 ppm (dominant) and −27 ppm corresponding to $H_2PO_4^-$, HPO_4^{2-}, PO_4^{3-} reveals that phosphorous is mainly incorporated as HPO_4^{2-} in the monolith (Figure 2D). Hence, we can draw the conclusion that the main composition of ZrP monolith is $Zr(HPO_4)_2$, which is in accordance with α-ZrP ($Zr(HPO_4)_2{\cdot}H_2O$).

Except for the composition of α-ZrP, ZrP macroporous monoliths with different Zr:P ratios have been synthesized. One of the well-known examples is NaSICON (Na super ionic conductor)-type ZrP ($MZr_2(PO_4)_3$, M = H, Li, Na, etc.) for its ion conductivity[33-35] and ultralow and even negative thermal expansion.[36,37] The extension of the method here to the synthesis of ZrP monoliths with different Zr:P ratios was carried out simply by changing the amount of phosphoric acid in the starting composition (Figure SI2, ESI†). Co-continuous macroporous ZrP monoliths with the NaSICON-type composition were successfully obtained by reducing the amount of phosphoric acid (Zr:P = 1:1.5, Figure SI2B, ESI†). A further decrease of the amount of phosphoric acid (Zr:P = 1:1) led to a coarsened structure with thick continuous skeletons (20-50 μm) and large amount of spherical particles in the pores, while a further increase (Zr:P = 1:4) led to the structure of particle aggregates. Further investigation into the synthesis of NaSICON-type ZrP monoliths and their properties is currently underway.

Shrinkage was observed during the drying process from wet gel to xerogel mainly due to the capillary force induced during the drying process together with the drying of the swollen polymers strongly bound to the ZrP skeletons, both of which led to elimination of the mesopores in the monolith. Supercritical drying using CO_2 was therefore used to bring the influence from the capillary force during the drying process to the minimum. Mesopores were found in the supercritically-dried ZrP monolith as a typical type IV nitrogen adsorption-desorption isotherm with a hysteresis of ink-bottle type mesopores together with the presence of micropores (Figure 3A-as-synthesized). Average mesopore size was 5 nm, confirmed by the BJH mesopore size distribution calculated from the adsorption branch (Figure 3B-as-synthesized). The presence of mesopores was also observed in the FE-SEM image, from which it can be speculated that the mesopores and micropores are mainly derived from the interstitials of small ZrP particles (Figure 4A). A consistent result was obtained from the TEM image showing a typical gel network formed by ZrP particles assembled together to form the monolithic architecture (Figure 4B). High BET surface area of about 600 $m^2\ g^{-1}$ (mesopore surface area 590 $m^2\ g^{-1}$ from the BJH method) was obtained. This is the highest surface area among those which have been reported (highest surface area reported

so far is about 500 m^2 g^{-1} in mesoporous ZrP particles obtained by surfactant-assisted precipitation,[38,39] Table 2).

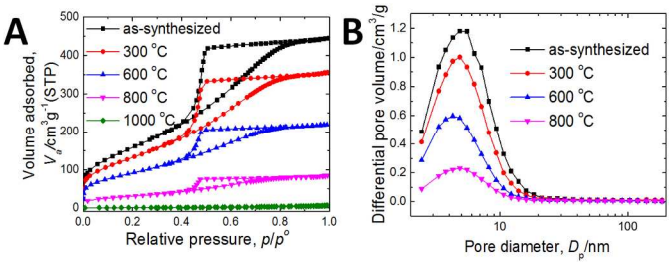

Figure 3. Nitrogen adsorption-desorption isotherms (A) and BJH mesopore size distributions (B) obtained from the adsorption branch of ZrP monoliths calcined at different temperatures.

Table 2 Pore characteristics of ZrP monoliths calcined at different temperatures.

Samples	S_{BET}/m^2 g^{-1}	V_p/cm^3 g^{-1}	D_p/nm
As-synthesized	600	0.68	5
300 °C	500	0.55	5
600 °C	340	0.34	4
800 °C	110	0.13	5

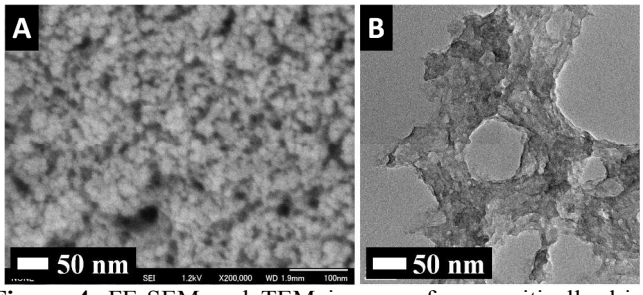

Figure 4. FE-SEM and TEM images of supercritically-dried ZrP monolith.

Thermal stability of porous morphologies and crystalline structure

Figure 5 and Figure 6 show the SEM images and crystalline structures of the ZrP monoliths calcined at different temperatures. The as-synthesized ZrP monolith shows low crystallinity indicated by the XRD pattern with low peak intensity (Figure 6A) and small crystallite size confirmed in the FE-SEM image (Figure 4), mainly due to the limited lattice growth by the coordinated PAAm and high viscosity of the solution. Calcination at low temperatures (< 1000 °C) did not affect the macroporous morphology but even lowered the crystallinity. Shrinkage was observed as a result of the thermal decomposition of polymers in the monolith and the condensation of hydroxyl groups. Calcination at 1000 °C induced the formation of ZrP_2O_7 without the collapse of the macroporous structure. The ZrP_2O_7 phase begins to decompose with the release of P_2O_5 when calcined at 1400 °C to form a mixed crystalline phases of ZrP_2O_7 (Zr:P = 1:2) and $Zr_2O(PO_4)_2$ (Zr:P = 1:1), which gave rise to the bimodal macroporous structure with small macropores forming in the gel skeletons (Figure 5F).

The effect of heat treatment on the mesoporosity of ZrP monoliths is shown in Figure 3A and 3B. Pore volume by the meso- and micropores gradually decreased as the calcination temperature increased from room temperature to 800 °C. This is mainly due to the condensation of hydroxyl groups at lower temperatures (< 800 °C), which decreases the volume of mesopores and micropores in the inorganic constituent. Calcination at 1000 °C gives rise to the growth of ZrP_2O_7 crystals which eliminates all the native micropores and mesopores, leading to the dense ZrP_2O_7 macroporous monolith (Figure 6). Detailed pore parameters of the monoliths calcined at different temperatures are listed in Table 2.

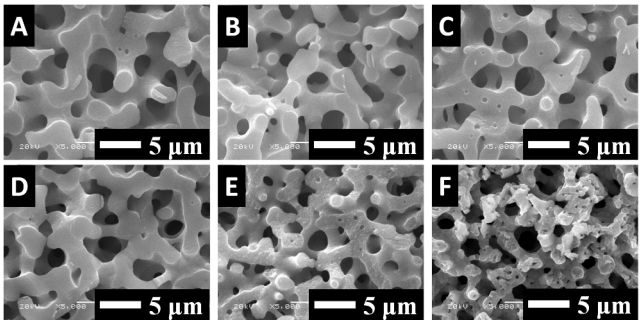

Figure 5. SEM images of ZrP monoliths calcined at different temperatures; as-synthesized (A), 300 °C (B), 600 °C (C), 800 °C (D), 1000 °C (E) and 1400 °C (F).

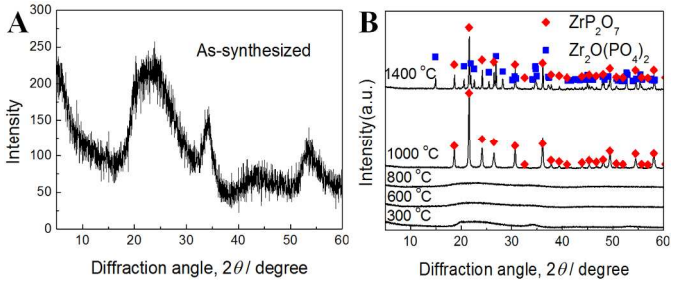

Figure 6. XRD pattern of as-synthesized ZrP monolith (A) and XRD patterns of ZrP monoliths (B) calcined at different temperatures.

ZrP monolith as ion exchanger

The ion exchange behavior of ZrP has been studied for decades. Most of the reports, however, concentrated on the kinetics and thermodynamics of the adsorption behavior of its different crystalline phases, in which particles were used in most of the cases.[2,40,41] Some studies reported about packing of ZrP particle slurry into a column.[42-44] Such columns could be used in a continuous flow set-up to remove toxic ions from liquids (aqueous solution in most of the cases). However, due to the high back pressure caused by the small through-pore size between the closely packed ZrP particles, the efficiency of the process is not satisfactory. Such drawbacks have been severely restricting the application of such techniques in the efficient treatment of waste water containing toxic ions. Compared with the particles, the hierarchically porous ZrP monolith we have synthesized in this research show more promising potential in the flow-through property, ensuring good contact of the reactants with the high surface area of the monolith. To check the mechanical properties of the monolith against the liquid pressure, Young's modulus of the as-synthesized monolith has been measured by uniaxial compression, and is found as high as 320 MPa (Figure SI3, ESI†). In order to efficiently treat

contaminated solution with a simple procedure, we have designed a syringe device shown in Figure 7 with the tight-fit ZrP monolith. The size of the monolith is the same as in the uniaxial compression test (Table SI1, ESI†).

In each run, 10 mL of about 10 mM metal salt solutions was introduced by the syringe pump at the flow rate of 0.2 mL/min through the syringe device to investigate the efficiency in ion adsorption even at high ion concentration. Altogether 8 kinds of metal were used including Ag^+, Cs^+, Sr^{2+}, Cu^{2+}, Zn^{2+}, Pb^{2+}, Cd^{2+} and Fe^{3+}, among which cesium and strontium are well known as radioactive metals (the metal source we used are not radioactive) while the rest are heavy metal ions commonly found in contaminated water. All the adsorption results are shown in Table 3. After adsorption by the ZrP monolith, the concentrations of these metal ions all decreased drastically, indicating the high efficiency of this device for the removal of these ions. In the case of Cu^{2+}, Pb^{2+} and Fe^{3+}, the concentrations were reduced to those that were lower than the detection limit (Cu^{2+} : < 1 ppb, Pb^{2+} : < 10 ppb, Fe^{3+} : < 1 ppb according to the specification document of the ICP-OES machine). In the cases of Cs^+, Sr^{2+} and Zn^{2+}, more than three magnitudes of concentration decrease were observed after the adsorption, while for Ag^+ and Cd^{2+}, the concentrations were reduced to less than 1/10 of the starting concentrations.

As a hydrated metal ion in the aqueous solution diffuses into the monolith, depending on the hydrated ionic radius, the ion will have to be dehydrated or partially dehydrated to allow itself further diffuse into the crystal lattice. The expenditure of the energy will be compensated by the strong electrostatic interaction between the cation and the fixed anionic site and the rehydration of the cation with water molecules diffused into the crystal lattice.[45] The lower adsorption efficiency of monovalent Ag^+ than Cs^+ could therefore be explained by its higher dehydration energy (Table 3). While in the cases of divalent and trivalent cations, although they are hydrated by more water molecules, the electrostatic interaction becomes dominant during the exchange process, resulting in the higher adsorption efficiency with Cd^{2+} as an exception. This exceptional behavior can be interpreted by the hard and soft acids and bases theory. As compared with other divalent cations, Cd^{2+} as a softer acid presents weaker interaction with the orthophosphate groups being a Lewis base, and consequently exhibits lower adsorption efficiency[7]. Overall, the results of ion adsorption demonstrate the high potential of such simple device inserted with a tightly fitted hierarchically porous ZrP monolith for water purification. Further details in the adsorption kinetics, capacity and recyclability are under investigation.

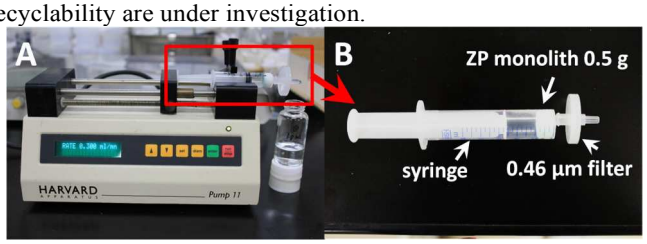

Figure 7. Photographs of the syringe pump under working (A) and syringe packed with a ZrP monolith (0.5 g) and a 0.46 μm filter (B).

Table 3 Detailed parameters of metal ions in aqueous solution and their concentrations before and after ion adsorption

Metal ions	Ag^+	Cs^+	Sr^{2+}	Zn^{2+}	Cu^{2+}	Pb^{2+}	Cd^{2+}	Fe^{3+}
Hydrated ionic radius[46]/Å	3.41	3.29	4.12	4.30	4.19	4.01	4.26	4.57
Number of H_2O molecules[47]	3.1	2.1	6.4	9.6	9.9	6.1	7.6	16.6
Free energy of hydration[46]/kJ mol^{-1}	-430	-250	-1380	-1955	-2010	-1425	-1755	-4265
Before adsorption/ppm	1070	1280	1100	290	740	2200	1150	620
After adsorption/ppm	63	1.5	0.3	0.4	< 0.001	< 0.010	87	< 0.001
Percentage of adsorption/%	94	99.9	> 99.9	99.9	> 99.9	> 99.9	92	> 99.9

Conclusions

Hierarchically porous ZrP monoliths with size-tunable co-continuous macropores have been synthesized from ionic precursors via sol-gel process accompanied by phase separation followed by supercritical drying. The main composition of the as-synthesized ZrP monolith is tunable as well from $Zr(HPO_4)_2$ (Zr:P = 1:2) to NaSICON-type ZrP (Zr:P = 1:1.5). Co-continuous macroporous structure is stable against heat treatment, which yields pure ZrP_2O_7 phase at 1000 °C, while treatment at even higher temperature (1400 °C) leads to further transformation. As a proof of concept, the as-synthesized ZrP monolith with high mechanical strength has been applied as a versatile material for different applications. The monolith has been tightly inserted into a syringe and applied to the removal of various metal ions in aqueous solution under a continuous flow condition, which shows promising results as a water purification device.

The synthetic method we have developed here would be further applied to the synthesis of other metal phosphates with hierarchically porous structure. The hierarchically porous ZrP and derivative monoliths may find their high potentials in more sustainable applications such as enrichment and recycling of precious metals and fuel cells.

Acknowledgements

The present work was financially supported by the Advanced Low Carbon Technology Research and Development Program (ALCA) from the Japan Science and Technology Agency (JST). N.B. is grateful to the Japan Society for the Promotion of Science for financial support.

Notes and references

[a] Department of Chemistry, Graduate School of Science, Kyoto University, Kitashirakawa, Sakyo-ku, Kyoto 606-8502, Japan.
E-mail: kanamori@kuchem.kyoto-u.ac.jp (K.K.),
kazuki@kuchem.kyoto-u.ac.jp (K.N.)
[b] Toyama National College of Technology, 13 Hongo-cho, Toyama 939-8630, Japan.
[c] GL Sciences, Inc. 237-2 Sayamagahara, Iruma, Saitama, 358-0032, Japan.

[d] Institute for Chemical Research, Kyoto University, Uji, 611-0011, Japan.

† Electronic Supplementary Information (ESI) available: SEM images of ZrP monoliths synthesized with different starting compositions, stress-strain curve of ZrP monolith from uniaxial compression test, detailed parameters of ZrP monolith for uniaxial compression test. See DOI: 10.1039/b000000x/

1 A. Clearfield and J. A. Stynes, *J. Inorg. Nucl. Chem.* 1964, **26**, 117.
2 A. Clearfield and S. D. Smith, *J.Colloid Interface Sci.* 1968, **28**, 325.
3 A. Clearfield, *J. Mol. Catal.* 1984, **27**, 251.
4 A. Clearfield and S. D. Thakur, *Appl. Catal.* 1986, **26**, 1.
5 Y. Z. Li, T. Kunitake, Y. Aoki and E. Muto, *Adv. Mater.* 2008, **20**, 2398.
6 A. Al-Othman, A. Y. Tremblay, W. Pell, S. Letaief, Y. Liu, B. A. Peppley and M. Ternan, *J. Power Sources* 2013, **224**, 158.
7 B. C. Pan, Q. R. Zhang, W. Du, W. M. Zhang, B. J. Pan, Q. J. Zhang, Z. W. Xu and Q. X. Zhang, *Water Res.* 2007, **41**, 3103.
8 S. Komarneni and R. Roy, *Nature* 1982, **229**, 707.
9 R. Chourasia, O. P. Shrivastava, R. D. Ambashta and P. K. Wattal, *Annual Nuclear Energy,* 2010, **37**, 103.
10 F. Kleitz, S. J. Thomson, Z. Liu, O. Terasaki and F. Schüth *Chem. Mater.* 2002, **14**, 4134.
11 U. Ciesla, S. Schacht, G. D. Stucky, K. K. Unger and F. Schüth *Angew. Chem. Int. Ed. Engl.* 1996, **35**, 541.
12 B. Z. Tian, X. Y. Liu, B. Tu, C. Z. Yu, J. Fan, L. M. Wang, S. H. Xie, G. D. Stucky and D. Y. Zhao, *Nat. Mater.* 2003, **2**, 159.
13 A. E. Kadib, R. Chimenton, A. Sachse, F. Fajula, A. Galarneau and B. Coq, *Angew. Chem.* 2009, **121**, 5069.
14 A. Sachse, A. Galarneau, F. D. Renzo, F. Fajula and B. Coq, *Chem. Mater.*, 2010, **22**, 4123.
15 V. Flexer, N. Brun, O. Courjean, R. Backov and N. Mano, *Energy Environ. Sci.*, 2011, **4**, 2097.
16 S. Ungureanu, H. Deleuze, C. Sanchez, M. I. Popa, R. Backov, *Chem. Mater.*, 2008, **20**, 6494.
17 N. Brun, A. Babeau-Garcia, M. Achard, C. Sanchez, F. Durand, G. Laurent, M. Birot, H. Deleuze, R. Backov, *Energy Enivron. Sci.*, 2011, **4**, 2840.
18 H. Minakuchi, K. Nakanishi, N. Soga, N. Ishizuka and N. Tanaka, *Anal. Chem.*, 1996, **68**, 3498.
19 K. Nakanishi and N. Tanaka, *Acc. Chem. Res.*, 2007, **40**, 863.
20 F. Sevc and C. G. Huber, *Anal. Chem.*, 2006, **78**, 2100.
21 D. S. Peterson, T. Rohr, F. Svec and J. M. J. Frechet, *Anal. Chem.*, 2002, **74**, 4081.
22 G. P. Hao, W. C. Li, D. Qian and A. H. Lu, *Adv. Mater.*, 2010, **22**, 853.
23 F. Carn, A. Derré, W. Neri, O. Babot, H. Deleuze and R. Backov, *New J. Chem.*, 2005, **29**, 1346.
24 K. Takeda, *Rev. Sci. Instrum.* 2007, **78**, 033103.
25 K. Takeda, *J. Magn. Reson.* 2008, **192**, 218.
26 C. Trobajo, S. A. Khainakov, A. Espina, J. R. García, *Chem. Mater.*, 2000, **12**, 1787.
27 J. Konishi, K. Fujita, S. Oiwa, K. Nakanishi, K. Hirao, *Chem. Mater.*, 2008, **20**, 2165.
28 Y. Kido, K. Nakanishi, A. Miyasaka, K. Kanamori, *Chem. Mater.*, 2012, **24**, 2071.
29 K. Nakanishi, *J. Porous Mater.*, 1997, **4**, 67.
30 L. Beneš, K. Melánová, J. Svoboda, V. Zima and M. Kincl, *J. Phys. Chem. Solids*, 2007, **68**, 803.
31 H. Kasgöz, S. Özgümüs and M. Orbay, *Polymer*, 2003, **44**, 1785.
32 A. Singhal, L. M. Toth, J. S. Lin and K. Affhotler, *J. Am .Chem. Soc.*, 1996, **118**, 11529.
33 A. Clearfield, B. D. Roberts and M. A. Subramanian, *Mater. Res. Bull.*, 1984, **19**, 219.
34 M. A. Subramanian, B. D. Roberts and A. Clearfield, *Mater. Res. Bull.*, 1984, **19**, 1471.
35 W. Wang, B. Jiang, L. W. Hu and S. Q. Jiao, *J. Mater. Chem. A*, 2014, **2**, 1341.
36 D. K. Agrawal, C. Y. Huang and H. A. Mckinstry, *Int. J. Thermophys.*, 1991, **12**, 697.
37 D. A. Woodcock, P. Lightfoot and C. Ritter, *Chem. Commun.*, 1998, 107.
38 Y. Sun, P. Afanasiev, M. Vrinat and G. Coudurier, *J. Mater. Chem.*, 2000, **10**, 2320.
39 P. Wu, Y. M. Liu, M. Y. He and M. Iwamoto, *Chem. Mater.*, 2005, **17**, 3921.
40 A. Clearfield and A. S. Medina, *J. Phys. Chem.*, 1971, **75**, 3750.
41 L. Kullberg and A. Clearfield, *J. Phys. Chem.*, 1981, **85**, 1585.
42 S. Ahrland, *J. Inorg. Nucl. Chem.*, 1971, **33**, 2229.
43 H. F. Maltez and E. Carasek, *Talanta*, 2005, **65**, 537.
44 E. Matoso, L. T. Kubota and S. Cadore, *Talanta*, 2003, **60**, 1105.
45 G. Eisenman, *Biophys. J.*, 1962, **2**, 259.
46 E. R. Nightingale Jr., *J. Phys. Chem.*, 1959, **63**, 1381.
47 Y. J. Marcus, Chem. Soc. *Faraday Trans.*, 1991, **87**, 2995.

Table of contents entry

Hierarchically porous zirconium phosphate monoliths have been synthesized and fabricated into a continuous flow setup for toxic metal ion adsorption.